SCI. MAR., 68 (3): 317-330 SCIENTIA MARINA 2004

Comparison of the two-dimensional directional wave spectra retrieved from spaceborne synthetic aperture radar images using the MPI scheme against directional buoy measurements*

NELSON VIOLANTE-CARVALHO[1,2] and IAN S. ROBINSON[1]

[1] Southampton Oceanography Centre, University of Southampton, European Way, Southampton, SO14 3ZH, UK.
[2] Present address: Marine Geology Lab LAGEMAR-UFF, Av. Litoranea s/n Boa Viagem, Campus Praia Vermelha 24210-310, Niteroi, Rio de Janeiro, Brazil. E-mail: nvc@igeo.uff.br

SUMMARY: Spaceborne Synthetic Aperture Radar (SAR) is to date the only source of two-dimensional directional wave spectra with continuous and global coverage when operated in the so-called SAR Wave Mode (SWM). Since the launch in 1991 of the first European Remote Sensing Satellite ERS-1, and more recently with ENVISAT, millions of SWM imagettes containing detailed spectral information are now available in quasi-real time. This huge amount of directional wave data has opened up many exciting possibilities for the improvement of our knowledge of the dynamics of ocean waves. However, the retrieval of wave spectra from SAR images is not a trivial exercise due to the nonlinearities involved in the mapping mechanism. In this paper we review the main features of the SAR ocean wave imaging mechanisms and give a detailed description of the Max-Planck Institut (MPI) retrieval algorithm which is running operationally at the European Centre for Medium-Range Weather Forecasts (ECMWF). Some examples of retrieved spectra are compared against directional buoy measurements obtained in deep water in the South Atlantic and against WAM spectra. The main characteristics of the MPI retrieval scheme are discussed and some of its deficiencies and strengths are identified.

Key words: wind wave, SAR spectrum, MPI scheme, SAR Wave Mode, ERS SWM imagettes.

RESUMEN: COMPARACIÓN DEL ESPECTRO DIRECCIONAL BIDIMENSIONAL DE OLEAJE OBTENIDO CON RADAR DE ABERTURA SINTÉTICA MEDIANTE EL ESQUEMA MPI RESPECTO A MEDIDAS CON BOYA DIRECCIONAL. – El radar de abertura sintética (SAR) operado desde satélite es actualmente el único medio que permite calcular espectros direccionales de oleaje bidimensionales de forma global y continua, cuando se opera en el denominado modo SAR de oleaje (SWM). Desde el lanzamiento en 1991 del primer Satélite Europeo de Observación de la Tierra (ERS-1), y más recientemente con el ENVISAT, millones de pequeñas imágenes SWM con información espectral detallada están disponibles en tiempo casi real. Esta enorme cantidad de datos de oleaje direccional ha abierto numerosas posibilidades a la mejora de nuestro conocimiento de la dinámica del oleaje oceánico. Sin embargo, la obtención del espectro de oleaje a partir de imágenes SAR no es un ejercicio trivial a causa de las no-linealidades que aparecen en el cálculo. En este artículo revisamos las principales características de los mecanismos de visualización del oleaje por parte del SAR, con una descripción detallada del algoritmo de recuperación del Instituto Max-Planck (MPI) que utiliza de forma operacional el Centro Europeo de Predicción del Tiempo a Medio Plazo (ECMWF). Algunos ejemplos de espectros obtenidos por este método son comparados con los obtenidos a partir de medidas realizadas por boyas de oleaje direccionales en aguas profundas del Atlántico sur.

Palabras clave: olas de viento, espectro de SAR, esquema MPI, SAR en modo oleaje, imágenes SAR SWM.

*Received January 7, 2003. Accepted February 27, 2004.

INTRODUCTION

Since the advent of spaceborne Synthetic Aperture Radar (SAR) in the early 1990s all weather ocean wave spectra are now available on a global basis and in quasi-real time. SAR is the only instrument so far deployed from satellites that is capable of measuring the two-dimensional directional wave spectrum and hence allowing the complete characterisation of a sea state. When operated in the SAR Wave Mode (SWM), the Advanced Microwave Instruments (AMI) on the European Remote Sensing satellites ERS-1 and ERS-2 acquire 10 x 5~km imagettes every 30 seconds, yielding an along track resolution of 200 km and a cross track resolution of 1000-2000 km. The 1500 imagettes that are collected daily bring enormous new possibilities for the study of wind generated waves providing global data with high temporal and spatial coverage.

From the practical point of view, this huge amount of spectral data has applications such as in optimisation of ship routing, wave climate atlases, offshore operations and coastal management. But this kind of information is also valuable for several scientific investigations. Improving the understanding of the dynamics of surface ocean waves is important for a better knowledge of, for example, climate dynamics (Janssen and Viterbo, 1996), transfer of momentum from the wind (Donelan, 1990) and exchange of gases through the air-sea interface (Csanady, 2001). The information extracted from SAR images has opened up new and exciting possibilities for wave modelers to assimilate observations of directional spectra into third generation wave models, an approach that has been hindered by the sparseness of directional wave measurements.

To retrieve the two-dimensional spectrum from SAR images is not a simple exercise. There are two main limitations in the images observed by SAR which demand great care in the process of deriving the wave spectrum. Firstly, there is a 180º directional ambiguity inherent in frozen images. This problem has been overcome with the launch of ENVISAT carrying the Advanced Synthetic Aperture Radar (ASAR), which uses successive images to solve the direction of propagation. Secondly, the SAR imaging mechanism is strongly nonlinear due to distortions induced by the orbital wave motions (the velocity bunching mechanism), causing degradation of the azimuthal (parallel to the satellite flight) resolution. The result of this distortion is that

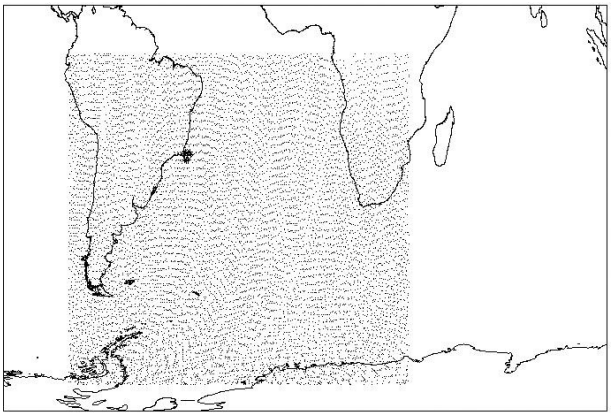

FIG. 1. – The selected area covers the South Atlantic from the Equator line to 72ºS and from 74ºW to 30ºE which is the lat-lon grid used for the wave model. Every dot represents one of the thousands of SAR Wave Mode imagettes during October in 1994 and the * are those closer than 150 km from the buoy.

there is a loss of information beyond a cut-off wavenumber and waves with wavelengths shorter than 150-200 m propagating in the azimuthal direction are not mapped onto the SAR image directly.

Therefore, to extract the wave spectrum from a SAR image spectrum requires additional information to solve the directional ambiguity and to recover the spectral information at the higher wavenumber band corresponding in general to the wind-sea part of the spectrum. This problem has been tackled by three different methods. The basic difference in their strategies lies in how they address the problem of reconstructing the directional spectrum beyond the high wavenumber azimuthal cut-off and hence filling in the spectral gap in the wind-sea part of the spectrum.

The first retrieval algorithm was developed at the Max-Planck Institut (MPI) by Hasselmann and Hasselmann (1991) and an improved version was published later by Hasselmann *et al*. (1996). They derived a closed expression for the mapping of a wave spectrum onto a SAR image spectrum, the forward mapping relation, together with a computationally efficient technique for inverting the mapping relation. The main idea behind the MPI scheme is to use a first-guess wave spectrum, in general from a wave model, and iteratively change its inverted SAR image spectrum to match the observed SAR image spectrum. They claim that the retrieval is independent of the first-guess which is used just to solve the directional ambiguity and to augment the spectrum beyond the azimuthal cut-off.

The second retrieval scheme to be proposed is a simplified version of the MPI scheme. Krogstad *et al*. (1994) applied a very similar approach but they

use a quasi-linear approximation of Hasselmann and Hasselamann's full nonlinear forward mapping relation. The nonlinearities in the mapping mechanism cause transfer of energy from the short wave components to the long wave components. Ignoring such nonlinearities by applying a quasi-linear approximation might cause spurious swell peaks when the SAR image spectrum is mapped back into the wave spectrum (see Hasselmann *et al*., 1985).

The Semi-Parametric Retrieval Algorithm (SPRA), the third retrieval scheme, was proposed by Mastenbroek and de Valk (2000), who employ additionally the wind information from the scatterometer that is operating simultaneously with the SAR. In this approach there is no need for a first-guess wave spectrum since they apply a parameterised wind sea spectrum and estimate its direction of propagation from the wind measurements. The drawback of this methodology is that the direction of propagation of swell is not determined and in general there is a spectral gap in the vicinity of the azimuthal cut-off, the delimitation between the part of the spectrum observed and not observed by SAR. In addition, if there is a swell shorter than 150-200 m its spectral component will not be detected by the retrieval scheme. The authors argue that their scheme is able to retrieve the wave components observed by SAR, which in the end is the information that is meant to be recovered. However, the most precise possible characterisation of the full two-dimensional spectrum is extremely desirable for two main reasons. First of all, it is much more convenient for practical purposes to handle the full spectrum rather than just its low frequency part. Secondly, the SAR mapping of the low frequency components is influenced by the shorter (high frequency) waves through the nonlinear transformation. Therefore, a better retrieval ought to be directly linked to a better representation of the high frequency components of the spectrum.

The quality of the retrieval schemes compared against independent directional data has not yet been demonstrated. Bauer and Heimbach (1999) compared the significant wave height extracted from ERS.1 SAR using the MPI scheme against Topex altimeter data. They found a good correlation between the two measurements but the comparison of an integral parameter does not provide much insight into the spectral capabilities of the retrieval. The spectral performance of the MPI scheme was compared against three years of WAM wave model spectra (Heimbach *et al.,* 1998) which were used themselves as a first guess for the inversion. Although the overall agreement was quite promising it was clear that an assessment against independent data, such as spectra from a directional buoy, would be more likely to point to any deficiencies of the method. More recently Voorrips *et al*. (2001) compared the MPI and the SPRA schemes against several non-directional buoys deployed mostly off the North American coast. In this work it became clear that both schemes show room for improvement, and that their main deficiencies lie in how to augment the spectral information beyond the azimuthal cut-off. However, one of the most striking characteristics of SAR data, their directional spectral information, was not considered. The main problem for such a comparison is a lack of available directional buoy data in deep water. The few directional buoys available to Voorrips *et al*. (2001) were not included in their analysis because they are moored in relatively shallow coastal waters, where one would expect a greater spatial variation of the wave parameters when compared to the more spatially homogeneous situations in the open sea.

The performance of the retrieval schemes has also been indirectly assessed through data assimilation exercises. The assimilation of spectral SAR data retrieved from the MPI scheme (Hasselmann *et al.,* 1997; Dunlap *et al*., 1998) and from the scheme by Krogstad *et al*., (1994) (Breivik *et al*., 1998) has shown no clear positive impact on the wave forecast. It is not clear from these assimilation experiments whether the lack of improvement in the forecasting is due to the SAR data and their retrieval or to the assimilation schemes. The nonlinear SAR imaging process involves a degree of uncertainty due to the complex mechanisms involved. Thus, a comparison of the retrieved spectra—meaning hereafter the final product to distinguish from the intermediate spectra obtained in the course of the inversion—against, for instance, directional buoy spectra has a twofold importance. On the one hand, such a comparison would allow us to clearly pinpoint deficiencies in the retrieval scheme; on the other hand, the linearly mapped low frequency band of the SAR image could give insights into the swell measured by the buoy.

The main goal of the present work is to supply a detailed investigation of the possibilities/limitations of mapping wind waves with a spaceborne SAR instrument using the MPI retrieval algorithm. The MPI scheme runs operationally at ECMWF and is the most broadly used algorithm to date implement-

ed in several institutions around the world. However very little is known about its performance assessed against independent measurements. We compare SAR wave spectra extracted from the MPI scheme against directional buoy spectra measured in the open ocean in the South Atlantic and against WAM spectra used as a first guess to the inversion. The main characteristics of the MPI retrieval scheme are presented together with a comprehensive review of the SAR modulation transfer functions. The structure of the paper is the following. In Section 2 the SAR imaging mechanisms are described in some detail while the MPI retrieval scheme is discussed in Section 3. Buoy and model data are presented in Section 4 and finally the results of the comparison and discussions are presented in Sections 5 and 6.

SAR OCEAN WAVE IMAGING MECHANISMS

It is quite remarkable that an instrument like SAR that emits microwave pulses able to penetrate no further than the very top skin layer of the ocean is capable of capturing in its back scattered pulse information about several oceanic features such as internal waves, shallow water bathymetry, current boundaries and surface gravity waves. In the explanation for what is, at first sight, a surprising response lie the principles of the SAR ocean wave imaging mechanism.

The ERS-1 satellite was launched in July 1991 into a sun-synchronous, polar, near-circular orbit operating at an altitude of about 785 km. Its payload consisted of an Active Microwave Instrument comprising a SAR (image and wave modes), a Wind Scatterometer, a Radar Altimeter and an Along Track Scanning Radiometer. In SAR image mode the instrument acquires 10 x 100 km images, but due mainly to onboard data storage limitations it can be operated only in the vicinity of a ground station. The SAR Wave Mode was introduced to yield global coverage of directional wave spectra since the much smaller images acquired in this mode are stored onboard and transmitted once per orbit to ground stations. Figure 1 shows the several thousand SAR Wave Mode imagettes acquired by ERS-1 during the period of one month over the South Atlantic. The resolution of the SAR Wave Mode imagette is similar to the SAR image mode, around 30 x 30 m. The spectrum consists of 12 x 12 polar wavenumber coordinates ranging from approximately 100 to 1000 m in wavelength (wave periods from 8 to 25 s) and covering a 180º sector, so with a directional resolution of 15º.

The ERS-1 SAR is a right-side-looking imaging radar operating at C-band (a frequency of 5.3 GHz). A SAR is an active all weather sensor transmitting its own radiation and receiving back part of the energy that was back scattered from the sea surface. The fraction of incident energy reflected back is called the radar cross-section and the radar modulation transfer function (MTF) is used to define the relation between the surface wave height and the amplitude of the variabilities of the radar cross-section. At the typical incidence angles used in SAR onboard satellites (23º from vertical for ERS-1) the electromagnetic waves emitted by SAR interact with short ocean surface waves in a process called the Bragg resonant scattering process (see for example Robinson, 1985, Chapter 12). The back scattered signal is proportional to the amplitude of these decimetric ocean waves denominated Bragg surface ripples. For ERS-1 the Bragg ripples have a wavelength of approximately 8 cm. These short waves are modulated by longer waves, such as a swell propagating on the surface or even internal waves propagating several metres in depth, which causes the longer waves to be visible on SAR images.

The imaging of ocean surface waves by SAR is based on a two-scale model (see for instance Komen *et al.,* 1994) consisting of the short waves whose wavelength is approximately half as long as the incident radar wavelength and the longer swell waves. The back scattered signal is affected by the slope of the long waves that changes the angle of view that the ripples present to the radar, the tilt modulation. Basically the amount of energy reflected back will be greater for the target plane (facet) facing towards the radar, while for the slope of the wave facing away the cross-section will be smaller. This mechanism is primarily sensitive to range travelling waves (perpendicular to the direction of satellite flight). Models of the Tilt MTF assume a Phillips k^{-4} (or f^{-5}) slope although the best representation for this high frequency decay exponent is still open to debate (see for instance Violante-Carvalho *et al.,* Buoy Observations of the Influence of Swell on Wind Waves in the Open Ocean, submitted to *Applied Ocean Research*, 2002 and references therein). The Tilt MTF is represented by

$$T_t = -k_r \frac{4\cot\theta}{1 \pm \sin^2\theta} e^{\frac{i\pi}{2}} \qquad (1)$$

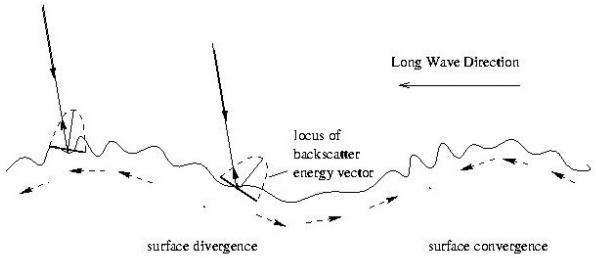

FIG. 2. – Representation of the tilt and hydrodynamic modulation processes. The dashed arrows indicate the component of the long-wave orbital velocity creating convergent and divergent patterns at the sea surface—the hydrodynamic modulation. The locus of backscatter energy vector illustrates the radar backscatter, which is strongest from the slope of the wave facing towards the radar and weakest facing away—the tilt modulation. Adapted from Robinson (1985).

where k_r is the component of the wavenumber vector in the range direction and q is the radar incidence angle. The ± sign represents vertical and horizontal polarisation respectively and hence the tilt MTF is strongest for horizontal polarisation. The maximum cross-section occurs on the face of the long wave - p/2 from the wave crest -as described by the phase in (1)

In addition the amplitude of the short waves is modulated by the long waves in a process called hydrodynamic modulation, which increases the energy of the Bragg waves near the swell crests and reduces the energy near the troughs. The currents induced by the orbital velocity field under the crest of the longer wave advect the Bragg waves, resulting in a convergent field which causes an increase in the amplitude of the ripples on the surface near the swell crest. Near the trough there is a corresponding reduction in ripple amplitude generating a pattern of increase and decrease of ripple amplitude connected to swell phase (Fig. 2). There are several equations to represent the hydrodynamic modulation; here we follow the form proposed in Hasselmann and Hasselmann (1991)

$$T_h = \frac{\omega - i\mu}{\omega^2 + \mu^2}(4.5)k\omega\left(\frac{k_r^2}{k^2} + Y_r + iY_i\right) \qquad (2)$$

The feedback coefficients Y_r and Y_i depend on the wind speed, μ is a damping factor and $w= 2pf$ where f is frequency. The best representation for the hydrodynamic modulation, the less well understood of the MTFs, is an issue under dispute. There is no phase dependence in (2), which implies that the maximum cross-section is on the crest of the long wave. The above equation expresses that the radar cross section depends on the local wind speed and on the long wave spectrum and, like the tilt modulation, cannot image azimuth travelling waves. Due to the less well understood representation of the hydrodynamic modulation, the incidence angle for the ERS-1 SAR was deliberately chosen to minimise the importance of this term in comparison with the better understood tilt modulation. Monaldo and Beal (1998), using a simplified version of (2), found a ratio between T_t/T_h equal to 6.1 for an incidence angle of 23º.

The linear Real Aperture Radar (RAR) modulation is composed of the hydrodynamic and tilt modulation and assumes that the target is stationary. Therefore, long waves travelling in the range direction are detected by SAR because of their effect on decimetric Bragg waves through the tilt and hydrodynamic modulations. However, long waves travelling in the azimuth direction cannot be detected in this way. The mechanism for the imaging of azimuth travelling waves is closely tied to the aperture synthesis process used to achieve a finer resolution in the azimuth direction. The along track resolution for an antenna of 10 m (like the one onboard ERS-1) without using the principle of aperture synthesis would be in the order of 5 km. Alternatively, for an azimuth resolution of 25 m an antenna of length 4 km would be necessary. The concept of aperture synthesis is used to improve the resolution without the need for augmenting the antenna's dimensions. The basic idea is to take advantage of the forward motion of the satellite using many returns of the target's reflection to build up a signal equivalent to that from a much larger antenna. Since the satellite's velocity is always changing in relation to the target, the instrument uses the time-dependent Doppler shift in frequency of the returned pulse to resolve the different target's position when performing the aperture synthesis.

Nevertheless, the sea surface is not a stationary target. The orbital velocity of the long ocean waves produces a vertical displacement of the location of the facets of small resonant waves. This vertical movement modifies the Doppler shift of the target, providing its own Doppler offset, implying that its apparent azimuthal position is displaced on the SAR image. The spatial mispositioning depends on the orbital velocity of the long waves, which is directly proportional to their mean frequency and significant wave height, and therefore sea state dependent. For ERS-1 a wave of mean frequency of say 0.1 Hz (wavelength of 156 m) and a significant wave height of 5 m would be displaced by more than 170 m in both azimuthal directions. The rising face of the wave is displaced in the positive azimuth direction,

whereas the falling face shifts in the negative azimuth direction. If this displacement, called velocity bunching, is small when compared to the wavelength of the long wave the effect is approximately linear. But if the displacement is of the same order as (or larger than) the wavelength of the long waves, which is the case for waves as in the previous example, the velocity bunching mechanism is highly nonlinear. These nonlinearities cause smearing of the image and an azimuthal fall-off with a high wavenumber azimuthal cut-off beyond which waves are not mapped into the SAR image plane. The azimuthal cut-off is sea state dependent and hence varies, but in general SAR cannot detect waves shorter than 150-200 m propagating in the azimuth direction. Therefore, the SAR imaging process can be thought of as a low-pass filter damping out the high wavenumber part of the spectrum.

The linear velocity bunching MTF is represented as

$$T_{vb} = \frac{R}{V} k_a \omega \left(\sin^2\theta \sin^2\phi + \cos^2\theta \right)^{1/2} \qquad (3)$$

where R is the distance between the radar and the ocean surface (slant range), V is the satellite ground track velocity, k_a is the component of the wavenumber vector in the azimuth direction and ϕ is the wave propagation angle with the satellite track ($\sin\phi = k_r/|\mathbf{k}|$). The phase of (3) depends on the sign of k_a; for positive values, or waves propagating in the same direction as the satellite, the maximum cross-section occurs at the wave crest. For negative values of k_a, or waves propagating antiparallel to the satellite, the minimum cross-section occurs at the wave crest. Reducing the ratio R/V, for instance with SAR on a lower altitude satellite, brings down the azimuth degradation caused by orbital motion and as a result the linear behavior of the velocity bunching mechanism applies over a larger wavenumber band.

It is still not clear which one of the three imaging mechanisms is the dominant one (see a comprehensive review in Hasselmann *et al.*, 1985). The mapping of a wave spectrum into an SAR image spectrum (and its inversion) has to take into account all the imaging mechanisms and the nonlinearities encountered at least in part of the spectrum. Hasselmann and Hasselmann (1991) developed a closed nonlinear integral transform for dealing with this problem which combines additional information, in general from wave models, with the incomplete information yielded by SAR images. The main feature of this integral transform is an exponential term that describes the azimuthal fall-off. The characteristics of the integral transform, together with a discussion of the MPI retrieval scheme, are presented in the next section.

THE MPI RETRIEVAL SCHEME

Hasselmann and Hasselmann noted that since the imaging mechanisms are quite well understood the forward mapping of an ocean wave spectrum into an SAR image spectrum can be computed numerically. However, the wave spectrum provided by SAR images is an incomplete spectrum. First of all, this is due to the directional ambiguity. Secondly, the nonlinearities caused by orbital motions result in an azimuthal high wavenumber cut-off and therefore waves shorter than 150-200 m propagating parallel to the satellite path are not imaged. In addition, due to spatial resolution and storage limitations waves shorter than approximately 70 m (period of approximately 7 s) propagating even in the range direction are not mapped onto the SAR image either. These constraints impose the use of a first guess to augment the spectral information. Hasselmann and Hasselmann recognised that because of this lack of information in the high wavenumber part of the spectrum not only was a forward mapping necessary but also a method for inverting this mapping relation must be devised which extends the missing spectral information with the use of a first guess wave spectrum.

The retrieval algorithm used in this work is the improved MPI scheme presented by Hasselmann *et al.* (1996). The mapping of an ocean wave spectrum $F(\mathbf{k})$ into an SAR image spectrum $P(\mathbf{k})$ (Hasselmann and Hasselmann, 1991) is a closed integral transform in the form

$$P(\mathbf{k}) = \exp\left(-k_a^2 \xi'^2\right) \sum_{n=1}^{\infty} \sum_{m=2n-2}^{2n} \left(k_a \beta\right)^m P_{nm}(\mathbf{k}) \qquad (4)$$

where $\exp(-k_a^2 \xi'^2)$ describes an exponential fall-off of the spectrum beyond an azimuthal cut-off wavenumber. This term can be thought of as a low-pass filter where the information beyond the cut-off is suppressed. The root mean square (rms) azimuthal displacement (ξ') is given by $\xi' = \upsilon_r \beta$ where β is the ratio of the slant range to the platform velocity R/V and υ_r is the orbital velocity. P_{nm} represents the Fourier transform of the auto and cross-covariance functions of the Real Aperture Radar image intensity and the orbital velocity. The indexes m and n indicate the order of nonlinearity with respect to the

velocity bunching mechanism and to the input wave spectrum respectively.

The full nonlinear mapping relation may be approximated by a quasi-linear mapping relation truncating (4) at $n = 1$, which is

$$P(\mathbf{k}) \sim \exp(-k_a^2 \xi'^2) P_1(\mathbf{k}). \qquad (5)$$

In the quasi-linear approximation the representation of the azimuthal cut-off term is retained but the nonlinearities in the mapping are not taken into account. The nonlinearities in the mapping mechanism cause transfer of energy from high to low azimuth wavenumbers, which are ignored using (5).

The MPI retrieval is performed in two steps. The first step or inner loop is the inversion of the mapping relation. An improved estimate of a given first guess wave spectrum is constructed through the minimisation of a cost function. The second step or outer loop is meant to reduce the spectral gap in the azimuthal cut-off. After the minimisation of the cost function the wave spectra of both the first guess and the observed SAR are partitioned into different wave systems and cross-assigned. The first guess wave systems are modified to conform to the observed SAR wave spectrum. In the following we discuss in more detail the two steps performed in the retrieval scheme.

The main idea behind the MPI retrieval scheme is to create a simulated SAR image spectrum from a first-guess wave spectrum through the mapping relation $P(\mathbf{k}) = \Phi(F(\mathbf{k}))$ (as specified by Equation 4). This first guess spectrum is compared to the observed SAR spectrum and the differences between the two spectra are minimised through the following cost function

$$J = \int \left[P(\mathbf{k}) - \hat{P}(\mathbf{k})\right]^2 \hat{P}(\mathbf{k}) d\mathbf{k} + \mu \int \frac{\left[P(\mathbf{k}) - \hat{P}(\mathbf{k})\right]^2}{\left\{B + \min\left[F(\mathbf{k}) - \hat{F}(\mathbf{k})\right]\right\}^2} d\mathbf{k} + \eta \frac{\left(\alpha\lambda_{cl}^2 - \alpha\hat{\lambda}_{cl}^2\right)^2}{\max\left\{\lambda_{cl}^4, \hat{\lambda}_{cl}^4\right\}} \qquad (6)$$

The first error term is a function of the deviation between the observed SAR spectrum $\hat{P}(\mathbf{k})$ and the fitted SAR spectrum $P(\mathbf{k})$. The second term expressing the deviations between the first-guess wave spectrum $\hat{F}(\mathbf{k})$ and the optimal fit wave spectrum $F(\mathbf{k})$ is necessary to solve the 180° directional ambiguity and to extend the information at high wavenumbers beyond the azimuthal cut-off. The factor m is set in order that the first-guess wave spectrum has a small influence in the part of the spectrum where SAR information is available but is great enough to solve the directional ambiguity ($\mu = 10^{-3}\hat{P}^3{}_{max}$), and B is a constant to prevent the denominator from vanishing. The third term in Equation (6) penalises the differences between the clutter cut-off length scale from the observed and simulated SAR spectrum represented by $\hat{\lambda}_{cl}$ and λ_{cl}. The value of the weighting factor ν is chosen to make the third error term of the same order of magnitude as the first term. To correct the errors in the cut-off, the scale parameter α is applied to the whole spectrum and not only to the low wavenumber part where there is SAR information. Hence α also modifies the high wavenumber components that contribute to the rms orbital velocities and consequently to the rms azimuthal displacement ξ'. Since λ_{cl} is determined by ξ' (both are proportional), a then affects $\lambda_{cl,}$ thus reducing the error between the observed and simulated cut-off.

Hence, the MPI scheme finds a retrieved wave spectrum by minimising a cost function which depends on the wave spectrum, the SAR spectrum and the azimuthal cut-off wavenumber. The full nonlinear mapping relation (4) is used to calculate the SAR image spectrum from a first-guess wave spectrum. However, the quasi-linear approximation (5) is applied to yield the direction of minimisation of the gradient of the cost function (6). The inversion is performed by the minimisation of the cost function J, which is achieved when the difference between two iterations is smaller than a specific value, in general after 6-10 iteration steps. The form of the spectrum is modified only up to the point where there is SAR spectral information, and beyond the cut-off wavenumber it retains the information from the first-guess wave spectrum. At this point an improved estimation of the first-guess wave spectrum is constructed which is used in the next step.

At every iteration the second step or outer loop replaces the input spectrum with the wave spectrum derived in the previous cycle. Therefore, the first-guess wave spectrum from the model is used only in the 0-th cycle, and after the first cycle of the outer loop its information is modified by new information based on the SAR image. The main reason for this additional loop is to resolve the discontinuities in the

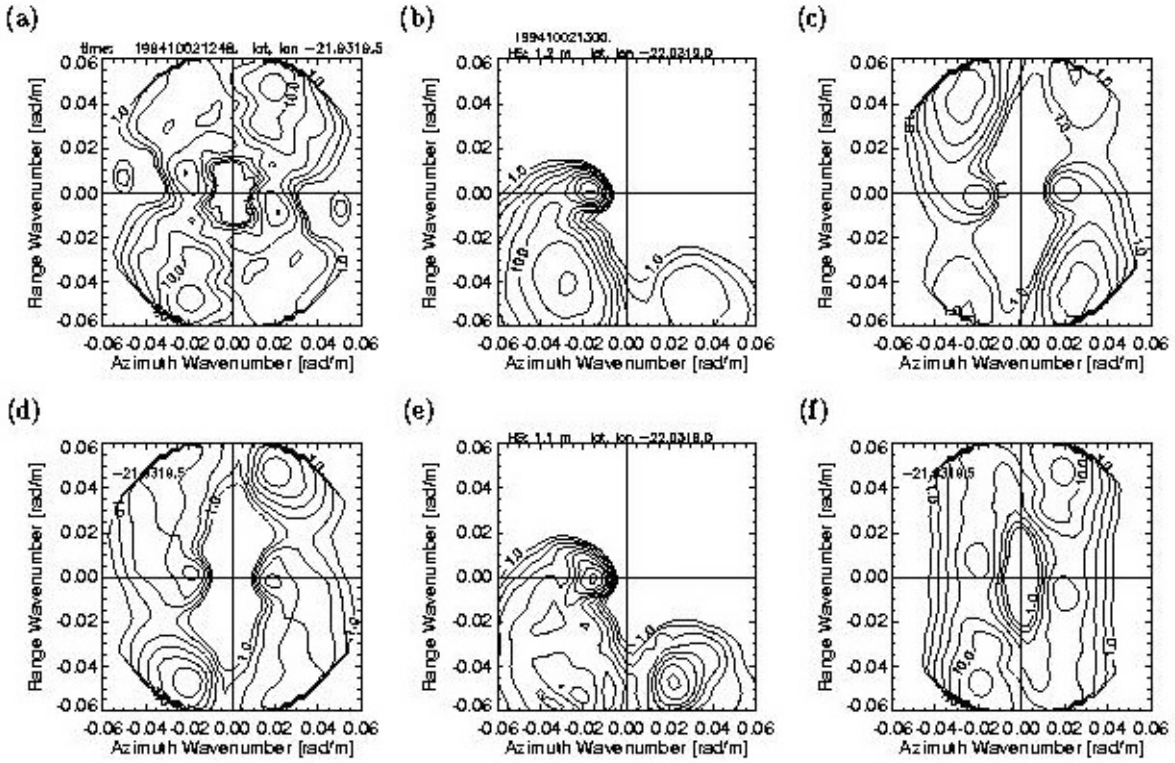

FIG. 3. – Example of the retrieval operation using the MPI scheme from 2 October 1994 1248 UT. Panel (a) is the observed SAR image, (b) is the a priori WAM wave spectrum, (c) is the first simulated SAR, (d) is the best simulated SAR of the iteration, (e) is the inverted wave spectrum and finally (f) is the retrieved SAR spectrum. All spectra in wavenumber domain with the x axis indicate azimuth direction, whereas the y axis indicates range direction.

vicinity of the cut-off wavenumber once the inversion modifies the spectrum up to this point. In addition, the second loop decouples the retrieval from the WAM first guess wave spectrum, implying that the retrieval (in a sense) is independent of the first guess.

The input two-dimensional spectrum is partitioned into different wave systems, that is swell, wind sea, old wind sea, each one represented by some wave parameters: significant wave height, mean frequency, spread width and direction. The shape of the wave systems does not change and only the wave height, mean frequency and direction are adjusted. Thus, the input spectrum maintains the characteristics of the original one, but the scales and directions are adjusted to conform to the observed spectrum. The program cycles five times around the outer loop and the updated spectrum from the previous loop is used as the input spectrum for the inversion in the next cycle.

Figure 3 shows one example of the retrieval operation. Panel (a) is the observed SAR image spectrum, whereas panel (b) is the a priori WAM wave spectrum which is used as a first guess in the 0-th iteration. Panel (c) is the first simulated SAR spectrum using the mapping relation $P(\mathbf{k}) = f(\Phi(\mathbf{k})$ of the first-guess wave spectrum (panel (b)). Panels (d) and (e) are respectively the best simulated SAR spectrum of the 0-th iteration and its inverted wave spectrum. The best inverted wave spectrum (e) is used as the input spectrum for the next iteration, and so on. Panel (f) is the retrieved SAR image spectrum from the iteration which yielded the smallest error between the observed spectrum and the input spectrum.

The MPI retrieval scheme is a complicated algorithm. The best way to identify its skill deficiencies and strengths is through comparisons against independent data. In the following sections the WAM model is described together with the in situ observations, and some comparisons are presented of retrieved ERS-1 SAR spectra against directional buoy data.

COLLOCATED DATA SET AND IN SITU OBSERVATIONS

WAM Data

In this work the directional spectra from WAM is used as a first-guess by the MPI retrieval scheme to remove the 180° ambiguity and to augment the wave

spectral information beyond the azimuthal cut-off wavenumber. A brief summary of the main characteristics of the third generation WAM model follows, but more detailed information is presented by WAMDI Group (1988); Günther *et al.* (1992); Komen *et al.* (1994) and on the web site at www.dkrz.de/forschung/reports/report4/wamh-1.html.

In contrast with second generation wave models, a third generation model such as WAM does not introduce assumptions about the shape of the spectrum (SWAMP Group, 1985). The 2D wave spectrum is determined by the integration of the transport equation:

$$\frac{D}{Dt}F \equiv \frac{\partial F}{\partial t} + \frac{1}{\cos\phi}\frac{\partial}{\partial \phi}\left(\dot{\phi}\cos\phi F\right) + \frac{\partial}{\partial \lambda}\left(\dot{\lambda}F\right) + \frac{\partial}{\partial \theta}\left(\dot{\theta}F\right) = S_{in} + S_{nl} + S_{ds} \quad (7)$$

where $F = F(f, \theta, \phi, \lambda, t)$, the two-dimensional wave spectrum is a function of the frequency f, the direction θ on a spherical grid of latitude ϕ and longitude λ and

$$\dot{\phi} = \frac{d\phi}{dt} \quad (8)$$

$$\dot{\lambda} = \frac{d\lambda}{dt} \quad (9)$$

$$\dot{\theta} = \frac{d\theta}{dt} \quad (10)$$

represent the rate of change of the position and direction along a great circle path for a wave packet in water of infinite depth. The source terms are represented by the wind input (S_{in}), the nonlinear transfer (S_{nl}) and the dissipation term (S_{ds}).

Since August 1993 ERS-1 altimeter wave height data have been assimilated by ECMWF into their WAM wave model using an optimal interpolation scheme. We are running a workstation version of the WAM without the implementation of any sort of data assimilation. This means that the outputs from the wave model used in this work are the direct result of integration of the energy balance equation (7) which makes the comparison of the model against buoy data much more meaningful. The ocean wave spectra are computed using the WAM cycle 4 every hour on a latitude-longitude grid with a spatial resolution of 1° covering the whole South Atlantic basin from the Equator line to 72ºS and from 74ºW to 30ºE, which totals 7488 grid points. Both the source and the advection terms have a time step of 12 minutes for all the 600 spectral components (25 frequencies and 24 directions). The spectrum is evaluated up to a high frequency cut-off, and beyond this point an f^{-5} tail is added with the same directional distribution as the cut-off region.

The wind input

The wind input is from the Atmospheric General Circulation Model (AGCM) which is run operationally by the European Centre for Medium-Range Weather Forecasts (ECMWF). Two different data sets were obtained from the British Atmospheric Data Centre (BADC). The first one is the ECMWF Re-Analysis (ERA) from 1991 to February 1994. The AGCM has a variable altitude resolution divided into 31 levels with a maximum altitude of 30 km; it has a latitude-longitude resolution of 1.125° and the wind field is computed every 6 hours. The second data set is the ECMWF Operational Analysis (from March 1994 to December 1995) and includes the same parameters with the same resolution as ERA. The wind field at 10 metres height (u_{10}) is used to drive the wave model. More details are presented on the web page http://www.badc.rl.ac.uk/.

In situ measurements

In Campos Basin—off the coast of Rio de Janeiro, Brazil—a heave-pitch-roll buoy was moored at the position 22º31'S and 39º58'W by the Brazilian Oil Company PETROBAS at a depth of over 1000 meters from March 1991 to March 1993 and from January 1994 to July 1995. This is the most important petrolic basin in Brazil (Fig. 4). More than 70 % of the petroleum prospected in the country comes from the tens of platforms located in this area. Every day several offshore operations take place in the region, which depends on the sea state, in particular on the surface waves. This is one of the most important regions in Brazil with huge urban concentrations and major commercial, industrial and touristic activities.

The equipment acquired three temporal series, i.e. the elevation (h) and two orthogonal inclinations (h_x and h_y) with a sampling rate of 1 Hz during 20 minutes every 3 hours. These temporal series are the starting point for the spectral analysis performed. Meteorological data (wind direction and intensity, air temperature and air pressure) and sea surface

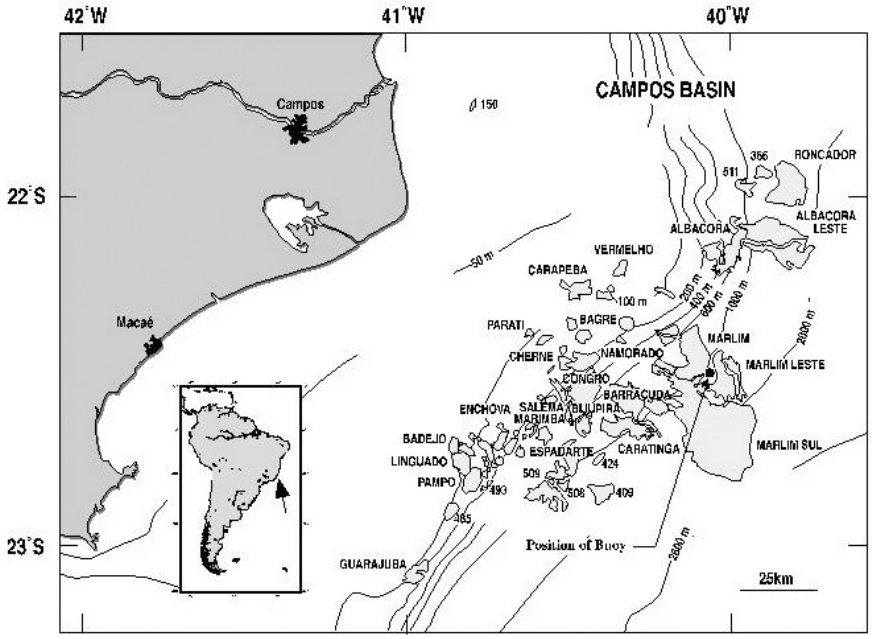

FIG. 4. – The South Atlantic and the position of the buoy in Campos Basin in the southeastern coast of Brazil. The shaded areas are the oil fields.

data (temperature, salinity and currents) were also acquired. The wave spectrum is calculated using classical Fourier analysis applying the Welch technique with a Hanning window and an overlap of 50%. The original register was segmented into 16 segments of 64 points (or in this case 64 seconds), implying 32 degrees of freedom and a frequency resolution of 0.015625 Hz. The spreading function is estimated using the Maximum Entropy Method (Lygre and Krogstad, 1986). See Violante-Carvalho *et al*. (2002) for more details about the buoy data processing.

Collocated data set

All SAR image spectra were collocated in space and time with WAM spectra at a maximum distance of 50 km (approximately half a WAM grid increment) and a maximum time separation of 30 minutes (half a WAM time increment). To validate the SAR inversions we chose a maximum time difference of 1.5 hour and a maximum distance of 150 km between buoy and SAR measurements. We are not using the quality control parameter from the MPI scheme to reject inversion results. The buoy is located around 150 km offshore at a depth of over 1000 meters. We chose these collocation criteria due to the relative temporal invariance and spatial homogeneity expected to be encountered in deep ocean areas.

Comparisons of retrieved ERS-1 SAR spectra against directional buoy data

For the present comparison of wave spectra extracted from ERS-1 SAR against directional buoy measurements and against WAM wave spectra we selected a few cases in the month of October 1994. The wave climate in Campos Basin can be explained on the grounds of the meteorological conditions encountered in the region (Violante-Carvalho, 1998). The semi-stationary South Atlantic high pressure centre with anti-cyclonic circulation is associated with descending air that usually creates good weather situations and with northerly or easterly winds generating wind sea with peak periods spanning from 3 to 5 s and a significant wave height of 0.25 to 1.25 m. Another wave system is also associated with the semi-stationary anti-cyclone, although it is not generated by the local wind. Due to the curved form of the isobars around the high pressure centre, a wave system is generated nearby by winds having directions in general 20 to 40º higher (clockwise) than the wind direction measured by the buoy. In this scenario a young swell with higher fetches and more energetic waves is generated with typical values of peak period ranging from 5 to 8 s and H_s from 0.5 to 2 m. Campos Basin is also highly affected all the year round by swell from the south quadrant, with typical peak periods ranging from 8 to 15 s and values of significant wave

height ranging from 0.5 to 2 m. More spatially and temporarily variable conditions are related to the passage of cold fronts with turning winds and gusts. However, during this period of the year the good weather scenario described above is more likely to be expected with a long swell propagating northward (and therefore in the azimuth direction since the SAR satellites fly in polar orbits) and a shorter, wind sea component propagating westward (in range direction).

Figure 5 is an example of retrieved spectra. Figure 5a shows the observed SAR image spectrum with the azimuthal cut-off wavenumber around 0.045 *rad/m* (or around 9.5 s). Two wave systems are clearly observed, a low wavenumber swell system propagating in azimuth direction and a partially observed wind sea system propagating in range direction. Figure 5b is the WAM first-guess wave spectrum and the retrieved SAR spectrum (5c) is in good agreement with the observed SAR spectrum. A typical scenario of good weather conditions measured by the buoy is presented in 5d, which is a swell system propagating northward and a wind sea propagating southwestward. The swell wave systems of the WAM first guess spectrum (5e) and of the retrieved SAR spectrum (5f) differ significantly, which demonstrates that the first guess is used only to solve the directional ambiguity. The wind-sea system is clearly overestimated both in 5e and 5f due to an overestimation of the wind speed yielded by the ECMWF model compared to the wind measured by the buoy. However, there is reasonably good agreement between the low frequency components measured by the buoy and those retrieved using the MPI scheme, which is the part of the spectrum directly measured by SAR.

Only the wave components in the low frequency part of the spectrum are visible on SAR images, whereas the high frequency information yielded by the retrieval is derived from the wave model. Therefore, only the swell systems are directly measured by SAR. Another example of good agreement between swell components measured by the buoy and retrieved by the MPI scheme is illustrated in Figure 6. Figure 6d is the directional spectrum measured by the buoy with a swell component propagat-

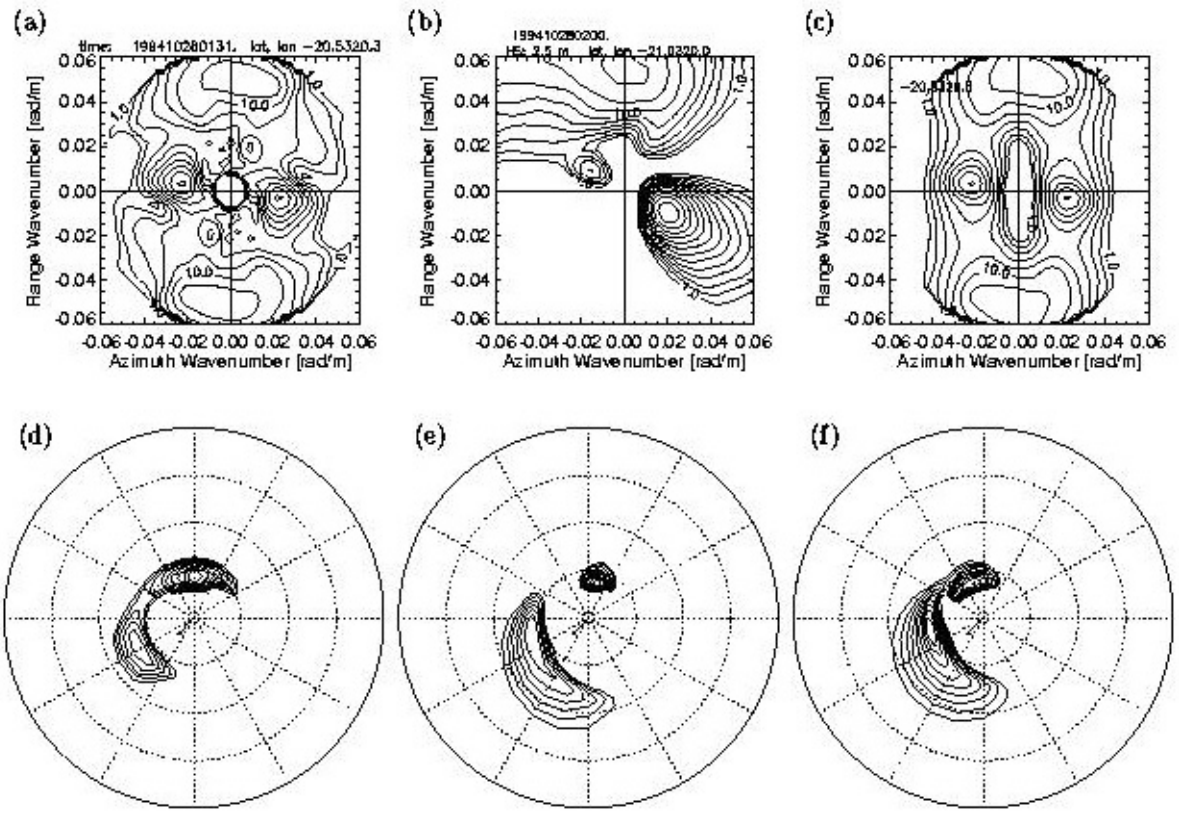

FIG. 5. – Example of the retrieval from 28 October 1994 0131~UT. Top row: panel (a) is the observed SAR image spectrum, (b) is the first guess WAM wave spectrum, and (c) is the retrieved SAR spectrum. Spectra in wavenumber domain with the x axis indicate azimuth direction, whereas the y axis indicates range direction. Bottom row: panel (d) is the buoy directional spectrum, (e) is the WAM first-guess spectrum and (f) is the retrieved SAR wave spectrum. Spectra in polar frequency-directional plots with the wind direction represented by the arrow in the centre. Circles denote frequency at 0.1 Hz interval from 0.1 Hz (inner circle) to 0.4 Hz (outer circle). Isolines are logarithmically spaced relative to the maximum value of the spectral energy density.

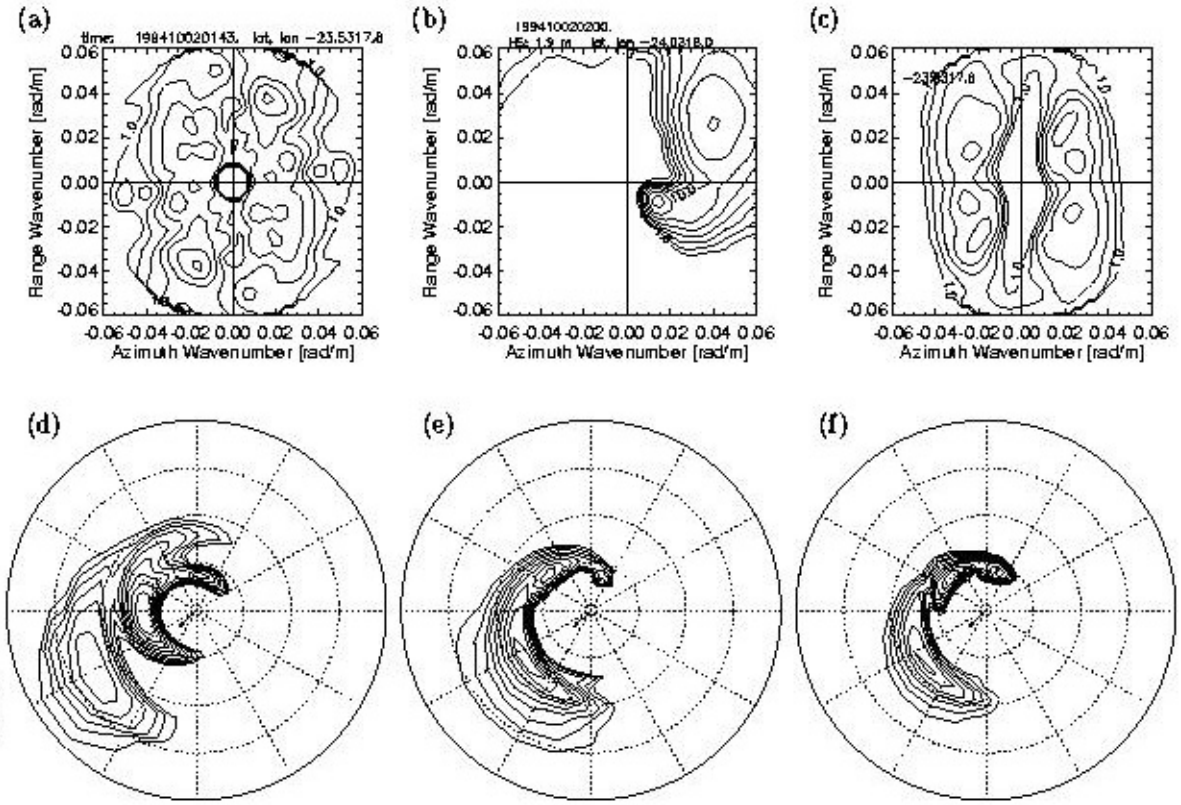

FIG. 6. – Example of the retrieval from 2 October 1994 0143~UT. Top row: panel (a) is the observed SAR image spectrum, (b) is the first-guess WAM wave spectrum, and (c) is the retrieved SAR spectrum. Spectra in wavenumber domain with the x axis indicate azimuth direction, whereas the y axis indicates range direction. Bottom row: panel (d) is the buoy directional spectrum, (e) is the WAM first guess spectrum and (f) is the retrieved SAR wave spectrum. Spectra in polar frequency-directional plots with the wind direction are represented by the arrow in the center. Circles denote frequency at 0.1 Hz interval from 0.1 Hz (inner circle) to 0.4 Hz (outer circle). Isolines are logarithmically spaced relative to the maximum value of the spectral energy density.

ing northward, a wind sea component propagating towards WSW and a young swell component propagating close to the wind sea both in direction and frequency (westward and 0.116 *Hz*). Although the wind sea component of the WAM spectrum (6e) is in good agreement with its counterpart in the buoy spectrum, the two spectra differ substantially in the low frequency components. The northward swell in 6d is barely detectable in 6e, whereas the direction of propagation of the young swell components differ by more than 30º, probably due to a mispositioning of the South Atlantic high pressure centre in the meteorological model. The retrieved spectrum (6f) clearly shows the northward swell component in very good agreement with the buoy observations in terms of direction of propagation, frequency and energy. The young swell component, which is located beyond the instrument cut-off and not mapped directly by SAR, still remains in disagreement with the buoy spectrum.

Table 1 presents some of the results derived from the retrieval scheme along with the wind data from the European Centre for Medium-Range Weather Forecasts and those measured by the buoy. Example 1 is the retrieved spectrum in Figure 5 and Example 2 is shown in Figure 6. Although the wind direction

TABLE 1. – Results derived from the retrieval scheme along with measured (buoy) and estimated (ECMWF) wind data. See text for more details.

	Example 1	Example 2
Date	October 28, 1994	October 2, 1994
Time, UTC	0131	0143
U_{10}, ecmwf (m/s)	11.07	11.12
θ, ecmwf (deg)	202	223
U_{10}, buoy (m/s)	3.94	7.66
θ, buoy (deg)	220	226
corr	0.90	0.82
λ, abs (m)	187.60	215.02
λ, ret (m)	204.94	> 400
Iterations	5	3
H_s, wam (m)	2.27	1.73
H_s, ret (m)	2.30	1.84
Mean Dir, wam (deg)	252	260
Mean Dir, ret (deg)	261	292
Mean Freq, wam (Hz)	0.11	0.14
Mean Freq, ret (Hz)	0.11	0.11

estimated from the ECMWF model is close to that measured by the buoy (q, ecmwf and q, buoy), there is an overestimation of the ECMWF wind speed at 10 m height in both examples (U_{10}}}, ecmwf and U_{10}, buoy). The correlation (corr) between the WAM (input) wave spectrum and the retrieved (ret) spectrum is also shown together with the number of iterations to find the best estimate. The azimuthal cut-off wavelengths observed (l, obs) and retrieved (l, ret) in Example 1 show reasonable results, whereas in Example 2 the cut-off adjustment was not attained. Significant wave height (H_s), mean propagation direction (mean~dir) and mean frequency (mean freq) are in close agreement in Example 1, whereas in Example 2 the quality of the retrieval is poorer with greater disagreement.

These two examples illustrate how the retrieved spectrum may yield useful information on the low frequency spectral components. However, the MPI algorithm is quite complex and a more extensive validation with in situ data presently underway will be necessary to pinpoint its deficiencies and its strengths (N. Violante-Carvalho and I. S. Robinson, Validation of ERS-1 SAR wave spectra against one year of directional buoy data, manuscript in preparation). Preliminary results show that for periods longer than 12 seconds (the part of the spectrum observed by SAR) the MPI method performs better than WAM for values of mean direction of propagation and for values of mean frequency. However, for periods shorter than 12 seconds its performance is worse, even considering the fact that the model is used as a first guess in the MPI scheme.

DISCUSSION

The MPI scheme was the first proposed and most widely used algorithm for retrieving directional wave spectra from SAR images. When it is operated in the SAR Wave Mode thousands of imagettes are available daily in quasi-real time with global and continuous coverage. This is a unique data set far beyond the capabilities of any other operational wave measurement system, both in terms of spatial and temporal coverage. We discuss in this paper the main strengths and weakneses of the retrieval scheme together with a review of the ocean wave-radar modulation transfer functions.

The retrieval of wave spectra from SAR images requires a first-guess wave spectrum to solve the inherent directional ambiguity of frozen images and to extend the spectral information beyond the high wavenumber cut-off caused by nonlinearities in the imaging process. Some examples of spectra retrieved with the MPI scheme are compared against directional buoy data and against the model spectra used as a first guess in the inversion. These examples highlight the strengths of the retrieval scheme, that is, the performance of the retrieval is better than the performance of the model for long (swell) components both in terms of direction of propagation and in terms of mean frequency.

This is exactly the compromise that must be achieved: one must stress the strength of one to compensate for the deficiency of the other. Third generation wave models such as WAM are known to describe very well the wind sea part of the spectrum, where there is no information mapped onto SAR images. On the other hand, the low frequency part is comparatively less well described by wave models, partially due to a poor understanding of the dissipation processes. The low wavenumber part of the spectrum is mapped quasi-linearly onto SAR images and hence the wave components are measured directly with additional information used only to solve the direction of propagation.

SAR data provide valuable information but must be considered with care because the retrieval schemes need to improve the performance of the wind sea retrieval. The three schemes proposed so far require a better representation of the high wavenumber part of the spectrum to fill in the spectral gap beyond the cut-off. However, as demonstrated in this paper, SAR does in fact yield useful information in the low frequency part of the spectrum.

ACKNOWLEDGEMENTS

We are grateful to PETROBRAS, the Brazilian Oil Company, for making available the buoy data. Violante-Carvalho was supported by the Brazilian research funding agency CNPq. Violante-Carvalho also acknowledges the support of the European COST714 Action, who sponsored the period that he spent as a Visiting Researcher working with Dr Susanne Lehner at the German Space Agency (DLR) in Oberpfaffenhofen, Germany. The short-term mission had the aim of solving several technical problems involved in the assimilation of wave data computed with the retrieval scheme of the Max-Planck Institut.

REFERENCES

Bauer and Heimbach. – 1999. Annual validation of significant wave heights of ERS-1 Synthetic Aperture Radar wave mode spectra using TOPEX/Poseidon and ERS-1 altimeter data. *J. Geophys. Res.,* 104(C6)13,345-13,357.

Breivik, L.A., M. Reistad, H. Schyberg, J. Sunde, H.E. Krogstad and H. Johnsen. – 1998. Assimilation of ERS SAR wave spectra in an operational wave model. *J. Geophys. Res*., 103 (C4)7887-7900.

Csanady, G.T. – 2001. *Air-Sea Interaction*. Cambridge University Press. 239 pp.

Donelan, M.A. – 1990. Air-sea interaction. In: B.L. Mehaute and D.M. Haines, editors, *The Sea*, volume 9 part A, pages 239-292.

Dunlap, E.M., R.B. Olsen, L. Wilson, S.D. Margerie and R. Lalbeharry. – 1998. The effect of assimilating ERS-1 fast delivery wave data into the north atlantic WAM model. *J. Geophys. Res*., 103(C4): 7901-7915.

Günther, H., S. Hasselmann and P. Janssen. – 1992. The WAModel cycle 4 (revised version). Technical report, Deutsches Klimarechenzentrum (DKRZ), Hamburg, Germany. Tech. Rep. 4.

Hasselmann, K. and S. Hasselmann. – 1991. On the nonlinear mapping of an ocean wave spectrum into a Synthetic Aperture Radar image spectrum and its inversion. *J. Geophys. Res*., 96(C6): 10,713-10,729.

Hasselmann, K., P. Lionello and S. Hasselmann. – 1997. An optimal interpolation scheme for the assimilation of spectral wave data. *J. Geophys. Res*., 102(C7): 15,823-15,836.

Hasselmann, K., R.K. Raney, W.J. Plant, W.Alpers, R.A. Schuchman, D.R. Lyzenga, C.L. Rufenach and M.J. Tucker. – 1985. Theory of Synthetic Aperture Radar ocean imaging: A MARSEN view. *J. Geophys. Res*., 90(C3): 4659-4686.

Hasselmann, S., C. Brüning, K. Hasselmann and P. Heimbach. – 1996. An improved algorithm for the retrieval of ocean wave spectra from Synthetic Aperture Radar image spectra. *J. Geophys. Res*., 101(C7): 16,615-16,629.

Heimbach, P., S. Hasselmann and K. Hasselmann. – 1998. Statistical analysis and intercomparison of WAM model data with global ERS-1 SAR wave mode spectral retrievals over 3 years. *J. Geophys. Res*., 103(C4): 7931-7977.

Janssen, P.A.E.M. and P. Viterbo. – 1996. Ocean waves and the atmospheric climate. *J. Climate*, 9: 1269-1287.

Komen, G.J., L. Cavaleri, M.A. Donelan, K. Hasselmann, S. Hasselmann and P.A.E.M. Janssen. – 1994. *Dynamics and Modelling of Ocean Waves*. Cambridge University Press, Great Britain. 532 p.

Krogstad, H.E., O. Samset and P.W. Vachon. – 1994. Generalizations of the non-linear ocean-SAR transform and a simplified SAR inversion algorithm. *Atmosphere-Ocean*, 32(1): 61-82.

Lygre, A. and H.E. Krogstad. – 1986. Maximum entropy estimation of the directional distribution in ocean wave spectra. *J. Phys. Oceanogr*., 16: 2052-2060.

Mastenbroek, C. and C.F. de Valk. – 2000. A semiparametric algorithm to retrieve ocean wave spectra from Syntetic Aperture Radar. *J. Geophys. Res.,* 105 (C2): 3497-3516.

Monaldo, F.M. and R.C. Beal. – 1998. Comparison of SIR-C SAR wavenumber spectra with WAM model predictions. *J. Geophys. Res*., 103 (C9): 18,815-18,825.

Robinson, I.S. – 1985. *Satellite Oceanography*. Ellis Horwood Ltd., Chichester, UK. 455 p.

SWAMP Group. – 1985. *Ocean Wave Modeling*. Plenum Press, New York (USA). 256 p.

Violante-Carvalho, N. – 1998. *Investigation of the Wave Climate in Campos Basin, Rio de Janeiro-Brazil and its Correlation with the Meteorological Situations -in Portuguese*. Master's thesis, Rio de Janeiro University- COPPE/UFRJ.

Violante-Carvalho, N., C.E. Parente, I.S. Robinson and L.M.P. Nunes. – 2002. On the growth of wind generated waves in a swell dominated region in the South Atlantic. *J. Offshore Mech. Arctic Engin*., 124: 14-21.

Voorrips, A.C., C. Mastenbroek and B. Hansen. – 2001. Validation of two algorithms to retrieve ocean wave spectra from ERS Synthetic Aperture Radar. *J. Geophys. Res*., 106(C8): 16,825-16,840.

WAMDI Group. – 1988. The WAM model-a third generation ocean wave prediction model. *J. Phys. Oceanogr*., 18: 1775-1810.

Scient. ed.: J. Font